Photofragmentation of the Fluorene Cation: I. New Experimental Procedure Using Sequential Multiphoton Absorption

Nguyen-Thi Van-Oanh,*,† Pierre Désesquelles,‡ Stéphane Douin,† and Philippe Bréchignac†

Laboratoire de Photophysique Moléculaire, CNRS, Fédération de Recherche Lumière Matière, Bât 210, Université Paris-Sud XI, F91405 Orsay Cédex, France, and Institut de Physique Nucléaire, IN2P3, Bât 100, Université Paris-Sud XI, F91405 Orsay Cédex, France

Received: December 8, 2005; In Final Form: February 28, 2006

The hydrogen-loss channel, induced by sequential multiphoton absorption, of the vapor-phase fluorene cation was investigated using a supersonic molecular beam and a time-of-flight mass spectrometer. The fluorene cation was prepared by resonantly enhanced multiphoton ionization. The ultimate goal of this experiment is the determination of the evolution of the dissociation rate constant in a wide energy range. In this paper, we give a description of the original experimental procedure, show that the absorption process is non-Poissonian, and determine the absolute photon absorption cross section.

Introduction

Polycyclic aromatic hydrocarbons (PAH) have been investigated much for astrophysical purposes during the past few decades. The major reason for this deals with the identification of the species responsible for a series of the IR emission bands observed in many astronomical objects.[1] These bands, which are well-known under the name of "unidentified infrared bands", have been observed with strong emission features at 3.3, 6.2, 7.7, 8.6, 11.3, and 12.7 μm. Following the coincidence of typical aromatic spectroscopic signatures with these observation bands, PAHs[2,3] have been considered as good candidates. Although the question of the exact nature of these PAHs has been addressed over the years and several improvements have also been made in related fields, no firm conclusion has been established.

From an intramolecular dynamics point of view, a PAH, under collisionless conditions, absorbs a UV photon issuing from stars (or a laser or a synchrotron, etc.); the molecule is thus electronically excited. Because internal conversion is a very efficient process in this class of large molecules (it occurs on a subnanosecond time scale), the molecular system then rapidly becomes highly vibrationally excited in the ground electronic state but stays rotationally and translationally cold. This transient heating mechanism of very small grains has been proposed first by Sellgren.[4] Two major possible channels for the de-excitation of these highly vibrationally excited molecules are either the infrared radiation emission or the fragmentation. The competition between these two relaxation channels depends on the excitation energy, molecular size, and nature of bondings in the molecule. Characterizing the vibrational spectroscopy of these PAHs as a function of the astrophysical relevant variables (role of the ionization, temperature influence, structure effects, etc.) provides a direct comparison with observation data. However, in connection with the stability of these PAHs in the interstellar medium, fragmentation studies must be considered. Thus, it is important to determine the evolution of the photodissociation rate versus internal energy with the ability to extrapolate the dissociation rate at small values (the estimated IR emission rate is about 10^2-10^3 s^{-1}). This allows one to establish the critical point energy, which plays a crucial role in ascertaining the PAH size distribution.

Mass spectrometry is especially suitable for photodissociation rate constant measurements. Many experimentalists have brought valuable information on the rate constants and on the branching ratios of the PAHs. Data derived from time-of-flight mass spectroscopy with a well-controlled energy deposit are available from the literature.[5,6] VUV wide-range energy synchrotron excitation has also been employed.[7,8] These techniques certainly offer valuable rate constant values at absorbed energies, which are generally located much above the dissociation threshold. Alternatively, continuous irradiation coupled with Fourier transform ion cyclotron resonance mass spectrometry is well suited for low energies,[9−12] especially nearby the activation energy, but the internal energy distribution in the molecule is not known. However, only a few works have led to the determination of the evolution of the rate constant versus energy.[13−18]

In this paper, we introduce a new experimental procedure for determining this evolution. We apply this method to fluorene cation $C_{13}H_{10}^+$ (see Figure 1), which presents a C_{2v} symmetry, to study its H-loss fragmentation. Fluorene has several astrophysical interests as a test molecule because it is one of the smallest PAHs and it contains a pentagonal ring.[19,20] The central carbon site is connected to two weakly out-of-plane hydrogen atoms. Thus, one of these two C−H bondings is broken easily. The second one then becomes in-plane and the strongest of all of the C−H bondings in the molecule. These features have been predicted using tight-binding molecular dynamics.[21]

This paper comes with a companion paper.[22] The former is devoted to the description of the new technique, the associated experimental setup, and the characterization of the excited molecular beam produced. The latter deals with the detailed description of the data analysis using the transition matrix method applied to the molecule fragmentation in order to determine the H-loss rate constant in an energy range. We

* Corresponding author. E-mail: vanoanh@lcp.u-psud.fr. Present address: Laboratoire de Chimie Physique, UMR 8000, CNRS, Bât 349, Université Paris-Sud XI, F91405 Orsay Cédex, France.

† Laboratoire de Photophysique Moléculaire.

‡ Institut de Physique Nucléaire.

10.1021/jp057164s CCC: $33.50
Published on Web 04/01/2006

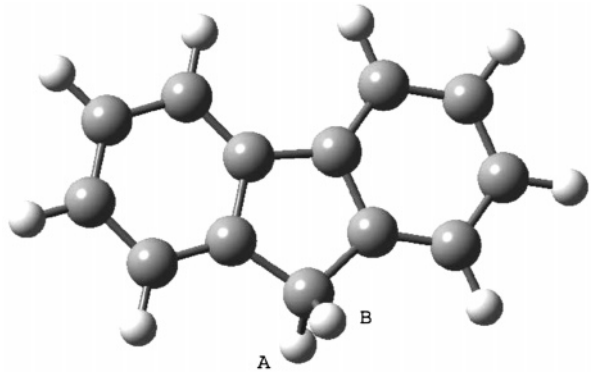

Figure 1. Graphical representation structure of the fluorene cation. The hydrogen atom at either position A or B is moved from the fluorene cation in the H-loss fragmentation channel.

believe that, beyond the physical results, the experimental method and the data analysis method might be useful for other experiments. Thus, the indispensable technical details will be given in both papers.

Methodology

To explain our method for the determination of the evolution of the fragmentation rates as a function of energy, we start by considering a very simplified reaction scheme consisting of a single photon absorption followed by a single yield fragmentation. In the following, of course, we will work with the actual multiphoton multifragment complex reaction scheme.

The intramolecular dynamics process can be detailed as follows: the initial parent molecule population ($N_p(t=0)=1$) first absorbs a photon with a given absorption rate, k_{abs}. The single photon excited state, N_p^*, is then populated. We make the assumption that the absorbed energy will be redistributed statistically among the ensemble of intramolecular modes more rapidly than both the dissociation process and the absorption of another photon. The evolution of the initial, excited, and product populations as a function of time will be governed by the kinetic law, given by

$$\underset{N_p}{C_{13}H_{10}^+} + h\nu \xrightarrow{k_{abs}} \underset{N_p^*}{C_{13}H_{10}^{+*}} \xrightarrow{k_{-H}} \underset{N_{-H}}{C_{13}H_9^+} + H \quad (1)$$

$$\frac{dN_p}{dt} = -k_{abs} N_p \quad (2a)$$

$$\frac{dN_p^*}{dt} = k_{abs} N_p - k_{-H} N_p^* \quad (2b)$$

$$\frac{dN_{-H}}{dt} = k_{-H} N_p^* \quad (2c)$$

In these equations, k_{abs} is the photoabsorption rate constant that is defined by

$$k_{abs} = \frac{\sigma}{S}\phi = \frac{\sigma}{S}\frac{\lambda}{hc}\frac{E_{laser}}{t_{pulse}} \quad (3)$$

where σ is the absorption cross section of the electronic state of the molecule. The photon flux, the number of photons per unit time, is noted ϕ (in s^{-1}). Furthermore, λ is the wavelength of the excitation photon, E_{laser} is the laser pulse energy, t_{pulse} is the laser pulse duration, and finally S is the laser spot surface.

Solving the first-order coupled differential equations (eqs 2a−c) gives the time-dependent populations:

$$N_p(t) = \exp(-k_{abs}\, t) \quad (4a)$$

$$N_p^*(t) = \frac{k_{abs}}{k_{-H} - k_{abs}}[\exp(-k_{abs}\, t) - \exp(-k_{-H}\, t)] \quad (4b)$$

$$N_{-H}(t) = \frac{1}{k_{-H} - k_{abs}}[k_{abs}\exp(-k_{-H}\, t) - k_{-H}\exp(-k_{abs}\, t)] + 1 \quad (4c)$$

From this set of equations, it can be seen that the populations evolve with time, t, and also depend on the absorption rate constant, k_{abs}. Because of the properties of the experimental setup (see further section), neither the pulse duration nor the mass spectrometer time-of-flight range can be modified. Nevertheless, it is possible to tune the photoabsorption rate constant. Indeed, this term depends on the wavelength of the absorbed photon and also on the flux of the photon source (see eq 3). As a result, the branching ratios can be expressed as a function of photon flux.

Moreover, by modifying the laser flux and the excitation wavelength, the number of absorbed photons can be increased. We now deal with a multiphoton process; the reaction scheme (eq 1) becomes more complex, and new fragment yields may open. This is the key point because this method gives access to the determination of a variety of rate constants. Note that both parameters, laser intensity and laser frequency, are controlled well and can be tuned easily. These particular features render our experimental facility very suitable for rate constant measurements.

We now focus on the fluorene cation. Spectroscopies of some electronic transitions are known accurately from earlier studies. The $D_3 \leftarrow D_0$ visible electronic transition and its absorption cross section have been characterized well in the vapor phase in our group.[23] This transition and the $D_4 \leftarrow D_0$ ultraviolet electronic transition values studied in matrices are also available from the literature.[24,25,10] In this work, we do not attempt to study all of the fragmentation pathways. Because of the nanosecond laser irradiation times used, only the H-loss fragment was dominantly present (see Figure 3).

The original experimental technique is based on the fact that the ionic molecules can absorb several photons successively during the laser irradiation, yielding methodologically for each laser frequency an equal number of microcanonical dissociation constants. It is important to note that the laser pulse width is much larger than the internal conversion time for such a large molecule[26] (typically about 300 fs); thus, with the number of absorbed photons being small,[22] the absorption process remains sequential. Figure 2 illustrates the intramolecular dynamics induced by the laser excitation leading to the fragmentation process. This figure also exhibits the way rate constants can be determined. Interestingly, the evolution of the dissociation rate versus internal energy will be obtained within a quite large energy range (proportional to the number of photon absorptions). It can finally be noted that the experimental technique and the data analysis method presented in this article and its companion paper[22] have some analogy with the work reported by Oomens et al.[27,28] in the infrared multiple-photon dissociation spectrocopy of PAH ions.

In the next two Sections, a detailed description of the experimental setup is given and raw mass spectrum data are shown. The absorption process will then be shown to be non-

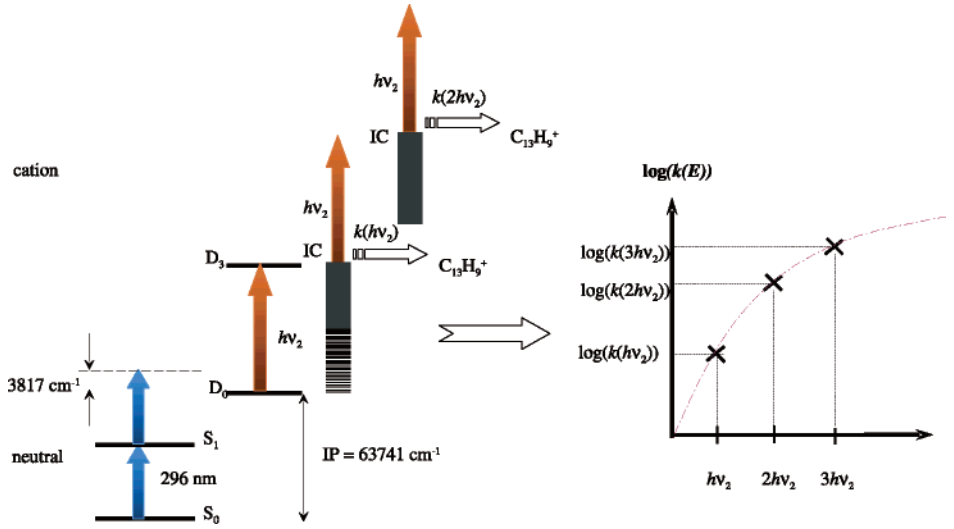

Figure 2. Schematic experimental principle for the photodissociation rate constants of the fluorene cation measurements. Ionization of the neutral fluorene was processed via the resonantly enhanced multiphoton ionization technique. Fragmentation is induced via a resonant absorption process, in this case the $D_3 \leftarrow D_0$ electronic transition. Internal conversion, which occurs at each stage of photon absorption, yields to increasing rate constants. Although this scheme illustrates the specific case of the $D_3 \leftarrow D_0$ electronic transition of the fluorene cation, it should be noted that this principle can be applied for any electronic transition available in a large molecule and more generally for any PAH.

Poissonian. The electronic absorption cross sections will be determined in the last Section.

Experimental Setup

The experimental apparatus has been described in detail elsewhere.[29,30,26] It consists of a microsecond time-of-flight mass spectrometer, a supersonic molecular beam, and a nanosecond laser system. Briefly, neutral vapor fluorene (produced by heating high-purity fluorene at 100 °C) was introduced into helium gas with a typical backing pressure of 4 bar. The mixture beam first traversed a pulsed valve with a pulse duration of 200 μs. Thus, the expansion conditions were reached to form a molecular supersonic beam from the valve orifice in a first vacuum chamber (operating pressure of $\sim 10^{-4}$ bar). The jet-cooled molecules then crossed through a very small skimmer, entering the second high vacuum chamber (operating pressure $\sim 10^{-6}$ bar). Here, the molecular beam met the outputs of two nanosecond pulsed dye lasers that were directed perpendicular to the beam. The first one ionized the neutral molecules by two resonant photons. The second one served to induce the fragmentation of these ionic species. The ultraviolet radiations used for both the ionization and fragmentation steps were obtained by nonlinear frequency doubling (KDP or BBO crystals). Both dye lasers and pump lasers used in this experiment are commercial products: Nd:YAG (type YG 481) operating at 532 nm pumped dye laser Quantel (type TDL III) and Excimer XeCl 308 nm pumped dye laser Lambda Physik (type FL2002). The role of the dye lasers (ionization or fragmentation) are completely interchangeable, depending on the electronic transition location of the molecule of interest. The whole system was operating at 10 Hz in repeat frequency.

The fragments were identified by a time-of-flight mass spectrometer. The resulting experimental information consists of mass spectra recorded with an oscilloscope as a function of the intensity of the second laser while holding its frequency constant. The same procedure was followed for two different laser frequencies. Finally, the evolution of the reactant-fragment proportions as a function of laser intensity can be deduced. In the following, the terms laser intensity or laser frequency will refer to the second laser used for the fragmentation step. Some advantages of this experimental setup are the following: the supersonic beam generates conditions similar to that in the interstellar medium (cold and collisionless) and nanosecond laser excitations are an adequate means to induce the fragmentation of the fluorene cation. This yields a sequential multiphoton absorption at various energies.

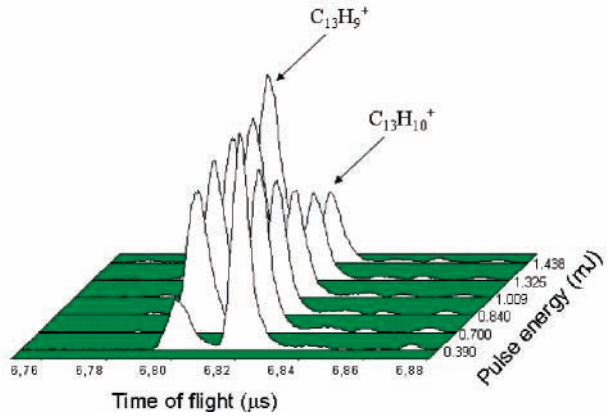

Figure 3. Set of experimental time-of-flight mass spectra of the fluorene cation for increasing values of laser pulse energy. Data recorded with the 3.4 eV photon excitation (corresponding to the $D_4 \leftarrow D_0$ transition).

Experimental Raw Results

Figure 3 shows a series of typical raw time-of-flight mass spectra collected at several different laser intensities. The laser frequency corresponding to the $D_4 \leftarrow D_0$ transition was used to induce the fragmentation.

It is seen immediately in this figure that there is an inversion of the parent-fragment populations. At very low laser intensity, the early H-loss signature is presented clearly. This fragment signal increases significantly while increasing the laser intensity, accompanied by a reduction of the parent signal. At high laser intensity (not shown in this figure), other fragments are observed such as multihydrogenated products and multiacetylene products. Yet, the intensities of these fragments are weaker than those of H-loss fragments. To simplify the analyses, in the following we regroup these fragments together to form a *unique* channel considered as leaked out from the reaction process and that will

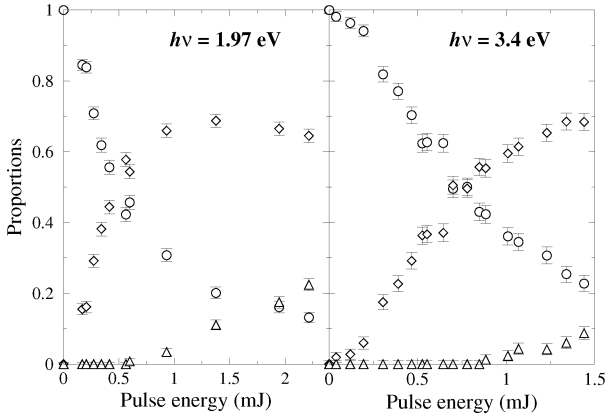

Figure 4. Measured relative integrated populations and their error bars as a function of laser pulse energy with photon excitations at 1.97 eV ($D_3 \leftarrow D_0$ transition, figure on the left) and at 3.4 eV ($D_4 \leftarrow D_0$ transition, figure on the right). The circle, diamond, and up triangle symbols exhibit parent, H-loss, and "leak" proportions, respectively.

be referred to simply as the *leak* channel in this work. Similar remarks can be made for the fluorene cation excitation at 1.97 eV.

Asymmetric Lorentz forms were applied to fit these mass spectra in order to determine the abundance of the fluorene parent cations and the fragment products by integrating each signal separately. Figure 4 plots the laser intensity-dependence of the relative proportions of the fluorene parent cation, H-loss fragment, and leak channel for experiments 1 and 2, respectively. The error bars have been taken into account for each experimental points via the following formula: $\Delta N = 0.05\sqrt{N(1-N)} + 0.01$.[31] They naturally include the uncertainties involved by the signal fitting procedure, the laser intensity measurement, and so on.

To give a thorough understanding of the data analysis involved in this experiment, we now discuss some important characteristic experimental parameters that were used in the kinetic equations. First of all, the ions have been prepared via the intermediate state of $S_1 \leftarrow S_0$ electronic transition of neutral fluorene (located at 4.16 eV (296 nm)[32] with a lifetime of 18 ns). The neutral fluorene can be ionized sufficiently by a one-color two-photon excitation scheme to overcome its ionization potential threshold lying at 7.91 eV.[25,33] This ionization process leads to a relatively low excess energy of 0.41 eV.

After ionization and fragmentation, the ions were deviated and accelerated. They are accelerated for 3 μs before entering a 4 μs time-of-flight region. These ions were then detected by a microchannelplate detector placed behind. Hence, the detection time is equal to 7 μs. Only the molecules resulting from fragmentation occurring during the acceleration phase will not populate the parent peak. Hence, the final time that has to be taken into account in the calculations is $t_{final} = 3$ μs. These time values have been checked rigorously by simulating the propagation of the fluorene cation in our mass spectrometer configuration. Finally, the irradiation time is equal to 6 ns and the temporal variation of the laser flux has been replaced by its mean value.

Poisson−Gauss Process

In this Section, we will determine if the photon absorption process is Poissonian, in which case the proportion of parent molecules having absorbed a given number of photons could be deduced directly from the absorption rate constant and from the laser pulse duration. This analysis is fully analytic (the details

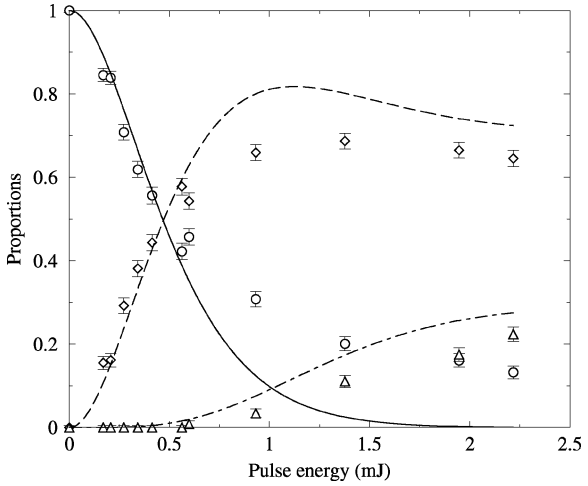

Figure 5. Solution of the Gaussian system (eq 9) under a priori constraints (the dissociation constants must be positive and must increase with the number of absorbed photons). The lines correspond to the optimization; the symbols (see conventions in Figure 4) stand for the experimental points.

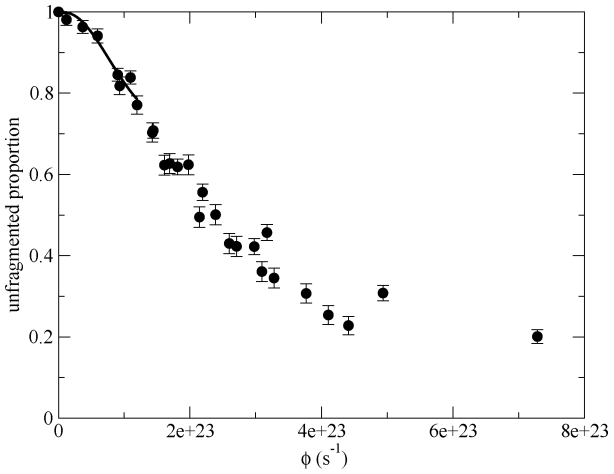

Figure 6. Proportion of detected unfragmented parent molecules as a function of the laser flux for $h\nu = 1.97$ eV (dots) and $h\nu = 3.4$ eV (open dots) photons. The curve shows the adjustments, to the experimental yields, of the formula (eq 5).

are given in the Appendix). It is based on the solving of a Gaussian system $\mathcal{NP} = \mathcal{S}$. The components of these matrices are, respectively, the proportion of parent molecules having absorbed a given number of photons for each experimental point (initial state matrix), the fragmentation branching ratios after absorption of given numbers of photons, and the experimentally measured molecular proportions (final state matrix). Hence, if one is able to evaluate the initial state matrix then the solving of the Gaussian system gives the values of the rate constants. The simplest method to determine the initial state matrix is to make the assumption that the absorption process is Poissonian.

Absorption Phase: Poisson Process. This assumption is true only if no fragmentation takes place during the laser pulse time and if the absorption constant does not depend on the number of absorbed photons.

In this case, the components of the $\mathcal{N}$ matrix can be determined (see eq 7 in the Appendix) and, as shown in Figure 7, the number of absorbed photons would vary between 0 and, for the highest intensity, 20.

Gauss Formalism of the Fragmentation Phase. The second phase runs from the end of the laser pulse to the moment when

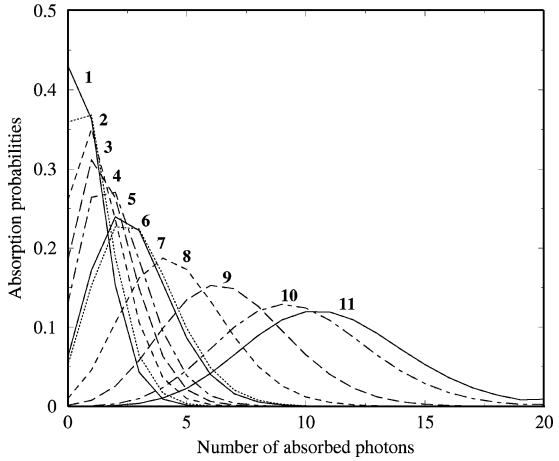

Figure 7. Distributions of the number of absorbed photons for the laser intensities corresponding to the 11 experimental measurements (1.97 eV). These curves result from two hypotheses: the absorption constant does not depend on the energy deposit, and fragmentation during the laser pulse duration is negligible.

the molecules are detected. The molecules can break up following two channels: hydrogen atom loss and leak. A parent molecule, after the absorption of given numbers of photons, will decay with given probabilities (matrix $\mathscr{P}$). Hence, one has to solve the Gaussian system and then deduce the rate constants from the probabilities. The method is developed in Appendix A. The results are shown in Figure 5.

In conclusion, the fragmentation is underestimated at low energy and largely overestimated at high energy. Indeed, to reproduce the rapid increase of the hydrogen-loss channel at low energy, the dissociation constants, for a small number of absorbed photons (for example, $j \leq 3$), must take high values. The constants for higher numbers of absorbed photons are forced to be even greater, which leads to an overestimation of the fragmentation probabilities at high energies. The only way to limit high-energy dissociation without modifying the probabilities at low energy is that the number of highly excited molecules is reduced. This is sufficient to say that the absorption process is not Poissonian. The saturation of the absorption at high energy can be induced by two, nonexclusive, causes: (1) the photon absorption process is limited by a significant decrease of the cross section for hot fluorenes and (2) the fragmentation process that takes place during the laser pulse is important enough at high energy so that it prevents the parent molecules from absorbing a large number of photons.

The latter possibility is already validated by the fact that the Poissonian analysis has led to dissociation constant values (for $j \geq 3$) largely greater than the inverse of the pulse time.

Cold Fluorene Cation Absorption Cross Section

The following discussion concentrates on the determination of the absolute absorption cross section of the fluorene cation between two electronic states involved in the $D_3 \leftarrow D_0$ and $D_4 \leftarrow D_0$ transitions. It will be used for the data analysis in a companion paper.[22]

The absorption cross section, σ, of a 1.97 eV photon ($\lambda =$ 630 nm) from the ground state by the fluorene cation has been measured by ref 23. But for the $D_4 \leftarrow D_0$ transition it is not known. A value of 0.6×10^{-16} cm^2 for the $D_3 \leftarrow D_0$ transition, with an error bar of 30%, was reported. We verify here its coherence with our experimental results.

We have found that, at low intensity, the Poissonian process is reasonably valid. Furthermore, it is also shown in ref 22 that the main fragmentation yield, in this intensity region, corresponds to parent molecules that have absorbed three photons. Thus, the proportion of parent molecules excited by three photons, at the end of the pulse time, can be approximated by $N_p^{3*} = (k_{abs}t_{pulse})^3\, e^{-k_{abs}t_{pulse}}/3!$. Hence, the measured population of unfragmented parent molecules follows the equation

$$N_p(\phi) = 1 - \frac{1}{3!}\left(\frac{\sigma t_{pulse}}{S}\phi\right)^3 \exp\left(-\frac{\sigma t_{pulse}}{S}\phi\right) \qquad (5)$$

where σt_{pulse} is a known constant. This formula can thus be adjusted to the experimental points (see Figure 6). The optimum value of S, given by a fitting procedure for a flux lower than 1.2×10^{23} s^{-1}, is 2.1 mm^2, which is in agreement with the experimental determination within uncertainties.[34]

Moreover, Figure 6 shows that, at low photon flux, the fragmentation follows the same trend for the two sets of data at different photon energies. This means that the absorption rate constant has very close values for both photon energies.

Conclusions and Perspective

A new experimental method has been proposed that is meant to determine the evolution of the dissociation rate with the deposit energy. The setup consists of a collimated supersonic molecular beam, a first laser being devoted to the ionization of the molecules by resonant two-photon absorption and a second nanosecond tunable laser allowing the excitation of the cations by multiphoton sequential absorption. The resulting fragments are discriminated by a time-of-flight mass spectrometer. The final experimental information consists of the proportions of the different fragmentation yields.

We have shown that the photoabsorption was a non-Poissonian process and that it was slowed at high laser intensity. This attenuation could result from two causes: fragmentation during the laser pulse and/or decrease of the absorption cross section for the hot fluorene cation. Because the absorption constant at high laser intensities is greater than the inverse of the pulse time, fragmentation is indeed in competition with absorption during the interaction with the laser.

In the energy region of validity of the Poissonian process, the adjustment of the parent molecule proportions at low laser intensities for the first experiment have confirmed the measurement of the absorption cross section for the cold fluorene cation made by ref 23 ($\sigma \approx 0.6 \times 10^{-16}$ cm^{-2} at $\lambda_2 = 630$ nm). A similar adjustment applied to the proportions of the second experiment ($\lambda_2 = 365$ nm) have led to the same, within uncertainties, absorption constant as that for the first experiment. Because the laser spot surfaces are close, this indicates that the cross sections are of the same order for both wavelengths. However, this method does not give information regarding the absorption cross section of the hot fluorene cation.

To determine the evolutions of the absorption and fragmentation constants with the deposit energy, we could solve analytically the kinetic equations for the absorption/fragmentation process. However, because the absorption/fragmentation scheme is not known a priori, the explicit solving of the sets of large numbers of differential equations for each possible scheme is an overwhelming task. The transition matrix method, introduced in a companion paper,[22] allows us to solve this problem while keeping the advantages of the analytical method, notably the possibility of taking into account the competition between absorption and fragmentation. Finally, the rate constant evolution

as a function of the deposit energy will be determined from the experimental data presented and characterized in the present paper.

Appendix: Poisson−Gauss Formalism of the Absorption and Fragmentation Process

The goal of this Appendix is to determine the rate constants under the hypothesis that, during the laser irradiation phase, the absorption process is purely Poissonian. The proportion of parent molecules having absorbed j photons are noted $N_p^{j^*}$. These quantities can be calculated by solving the following differential system:

$$\forall j, \quad \frac{dN_p^{j^*}}{dt} = k_{abs}\,(N_p^{(j-1)^*} - N_p^{j^*}) \tag{6}$$

The same result can be obtained directly writing that the j photon absorption probability is given by the Poisson law, which parameter is equal to the mean number of absorbed photons ($\langle n_{h\nu}\rangle = k_{abs}t_{pulse} = \sigma E_{laser}/(h\nu S)$):

$$\forall j, \quad N_p^{j^*} = \frac{(k_{abs}\,t_{pulse})^j}{j!}\,e^{-k_{abs}t_{pulse}} \tag{7}$$

The energy deposit distribution can thus be calculated for each value of the laser intensity, that is, for each experimental measurement (see Figure 5). The mean number of absorbed photons depends only, at a given wavelength, on the energy contained in the laser pulse.

After the laser pulse, the molecules are accelerated and then detected. They can break up but cannot gain excitation energy. A parent molecule, after the absorption of j photons, will decay with probabilities $p_{-H}^{j^*}$ and $p_{leak}^{j^*}$ along the two channels. The resulting proportions of detected molecules will be noted $N_{-H}^{j^*}$ and $N_{leak}^{j^*}$ (we insist that the j^* refer to the number of photons absorbed by the *parent* molecule prior to fragmentation). The three experimentally measured molecular proportions can thus be written as

$$N_{-H} = \sum_j N_{-H}^{j^*} = \sum_j N_p^{j^*} p_{-H}^{j^*}$$

$$N_{leak} = \sum_j N_{leak}^{j^*} = \sum_j N_p^{j^*} p_{leak}^{j^*}$$

$$N_p = 1 - N_{-H} - N_{leak} \tag{8}$$

Considering all of the experimental points, the two former equations can be written under a matrix form as

$$\mathcal{E} = \mathcal{N}\mathcal{P} \tag{9}$$

The terms of matrices $\mathcal{N}$ (eq 7) and $\mathcal{E}$ (experimental proportions) are known; thus, the decay probabilities can be obtained by solving this system. Whatever the dimensions of the $\mathcal{N}$ matrix, the least-squares solution is given by

$$\mathcal{P} = (\mathcal{N}^T\mathcal{N})^{-1}\,\mathcal{N}^T\mathcal{E} \tag{10}$$

where the superscript T denotes the transpose of the matrix. From these probabilities, we can deduce the corresponding dissociation constants. Indeed, the differential system that describes the fragmentation process is the following:

$$dN_{-H}^{j^*} = k_{-H}^{j^*} N_p^{j^*}\,dt$$

$$dN_{leak}^{j^*} = k_{leak}^{j^*} N_p^{j^*}\,dt$$

$$dN_p^{j^*} = -(k_{-H}^{j^*} + k_{leak}^{j^*})\,N_p^{j^*}\,dt \tag{11}$$

Furthermore, the components of the $\mathcal{P}$ matrix are, by definition

$$p_{-H}^{j^*} = \frac{N_{-H}^{j^*}(t_{final})}{N_p^{j^*}(t_{pulse})}$$

$$p_{leak}^{j^*} = \frac{N_{leak}^{j^*}(t_{final})}{N_p^{j^*}(t_{pulse})} \tag{12}$$

Noting $p_p^{j^*} = 1 - p_{-H}^{j^*} - p_{leak}^{j^*}$, the proportions, at final time, of unfragmented fluorene cations, the solution of the system is[36]

$$k_{-H}^{j^*} = p_{-H}^{j^*}\frac{\ln p_p^{j^*}}{(t_{final} - t_{pulse})(p_p^{j^*} - 1)}$$

$$k_{leak}^{j^*} = p_{leak}^{j^*}\frac{\ln p_p^{j^*}}{(t_{final} - t_{pulse})(p_p^{j^*} - 1)} \tag{13}$$

In our case, the Gaussian system is underdetermined. A mere solving would give a solution that fits the experimental points exactly but shows large, unphysical fluctuations between the points. We have tried to regularize the solution by adding "artificial" experimental points using a smooth spline interpolation so that the Gaussian system becomes squared. The fluctuations are removed, but the system remains underdetermined and the resulting rate constants are unphysical (some take negative values).

To solve this underdetermination problem, a priori constraints were imposed to the $\mathcal{P}$ matrix, that is, the dissociation constants must take positive values that increase with the energy deposit. The system is solved by residue minimization. As shown in Figure 5, the adjustment to the experimental points is very bad. Therefore, one can conclude that the absorption process is not Poissonian over the whole energy range.[35] Following the same method, we have verified that the process was reasonably Poissonian up to a pulse energy of about 0.5 mJ.

References and Notes

(1) The other main motivations for the study of the PAHs are connected to their potential effects on environment and on human health.
(2) Léger, A.; Puget, J. *Astron. Atrophys.* **1984**, *137*, L5.
(3) Allamandola, L.; Tielens, A.; Barker, J. *Astrophys. J. Ser.* **1985**, *290*, L25.
(4) Sellgren, K. *Astrophys. J.* **1984**, *277*, 623.
(5) Klippenstein, S.; Faulk, J. D.; Dunbar, R. *J. Chem. Phys.* **1993**, *98*, 243.
(6) Ho, Y.; Dunbar, R.; Lifshitz, C. *J. Am. Chem. Soc.* **1995**, *117*, 6504.
(7) Jochims, H.; Rühl, E.; Baumgärtel, H.; Tobita, S.; Leach, S. *Astrophys. J.* **1994**, *420*, 307.
(8) Jochims, H.; Baumgärtel, H.; Leach, S. *Astrophys. J.* **1999**, *512*, 500.
(9) Boissel, P.; Parseval, P.; Marty, P.; Lefèvre, G. *J. Chem. Phys.* **1997**, *106*, 4973.
(10) Dibben, M.; Kage, D.; Szczepanski, J.; Eyler, J.; Vala, M. *J. Phys. Chem. A* **2001**, *105*, 6024.

(11) Ekern, S.; Marshall, A.; Szczepanski, J.; Vala, M. *Astrophys. J.* **1997**, *L39*, 488.
(12) Ekern, S.; Marshall, A.; Szczepanski, J.; Vala, M. *J. Phys. Chem. A* **1998**, *102*, 3498.
(13) Proch, D.; Rider, D.; Zare, R. *Chem. Phys. Lett.* **1981**, *81*, 430.
(14) Boesl, U.; Neusser, H.; Weinkauf, R.; Schlag, E. *J. Phys. Chem.* **1982**, *86*, 4857.
(15) Kühlewind, H.; Neusser, H.; Schlag, E. *J. Phys. Chem.* **1984**, *88*, 6104.
(16) Kühlewind, H.; Kiermeier, A.; Neusser, H. *J. Chem. Phys.* **1986**, *85*, 4427.
(17) Kiermeier, A.; Ernstberger, B.; Neusser, H.; Schlag, E. *J. Phys. Chem.* **1988**, *92*, 3785.
(18) Neusser, H. *J. Phys. Chem.* **1989**, *93*, 3897.
(19) Moutou, C.; Verstraete, L.; Léger, A.; Sellgren, K.; Schmidt, W. *Astron. Astrophys.* **2000**, *354*, L17.
(20) Kerckhoven, C. V.; Hony, S.; Peeters, E.; Tielens, A.; Allamandola, L.; Hudgins, D.; Cox, P.; Roelfsema, P.; Voors, R.; Waelkens, C.; Waters, L.; Wesselius, P. *Astron. Astrophys.* **2000**, *357*, 1013.
(21) Van-Oanh, N.-T.; Parneix, P.; Bréchignac, P. *J. Phys. Chem. A* **2002**, *106*, 10144.
(22) Van-Oanh, N.-T.; Désesquelles, P.; Bréchignac, P. *J. Phys. Chem. A* **2006**, *110*, 5599.
(23) Pino, T.; Bréchignac, P.; Dartois, E.; Demyk, K.; d'Hendecourt, L. *Chem. Phys. Lett.* **2001**, *339*, 64.
(24) Shida, T. *Electronic Absorption Spectra of Radical Ions*; Elsevier: Amsterdam, 1988.
(25) Szczepanski, J.; Banisaukas, J.; Vala, M.; Hirata, S.; Barlett, R.; Gordon, M. *J. Phys. Chem. A* **2002**, *106*, 63.
(26) Pino, T.; Boudin, N.; Bréchignac, P. *J. Chem. Phys.* **1999**, *111*, 7337.
(27) Oomens, J.; Tielens, A.; Sartakow, B.; von Helden.; Meijer, G. *Astrophys. J.* **2003**, *591*, 968.
(28) Oomens, J.; Moore, D.; Meijer, G.; von Helden, G. *Phys. Chem. Chem. Phys.* **2004**, *6*, 710.
(29) Douin, S.; Fillion, J.-H.; Bonneau, M.; Bréchignac, P.; Furio, D.; Gauyacq, D.; Horani, M.; Shafizadeh, N. *Chem. Phys. Lett.* **1993**, *216*, 215.
(30) Bréchignac, P.; Pino, T. *Astron. Astrophys.* **1999**, *343*, L49.
(31) Van-Oanh, N.-T. *Spectroscopie et stabilité des hydrocarbures aromatiques polycycliques dans les conditions du milieu interstellaire* Ph.D. Thesis, Université Paris XI, 2003.
(32) Kauffman, J.; Côté, M.; Smith, P.; Donnald, J. M. *J. Chem. Phys.* **1989**, *90*, 2874.
(33) Maier, J.; Turner, D. *J. Chem. Soc., Faraday Trans. 2* **1973**, *69*, 196.
(34) This approximated calculation also allows one to understand the small bolsters at the very beginning of the decrease of the parent molecule proportion for both experiments. It is due to the molecule fragmentation threshold.
(35) Mehlig, K.; Hansen, K.; Heden, M.; Lassesson, A.; Bulgakow, A.; Campbell, E. *J. Chem. Phys.* **2004**, *120*, 4281.
(36) These equations are valid more generally regardless of the number of decay channels.